

Multicolour micropatterning of thin films of dry gels

RAFAL KLAJN, MARCIN FIALKOWSKI, IGOR T. BENSEMANN, AGNIESZKA BITNER, C. J. CAMPBELL, KYLE BISHOP, STOYAN SMOUKOV AND BARTOSZ A. GRZYBOWSKI*

Department of Chemical Engineering, Northwestern University, 2145 Sheridan Rd, Evanston, Illinois 60208, USA

*e-mail: grzybor@northwestern.edu

Published online: 19 September 2004; doi:10.1038/nmat1231

Micropatterning of surfaces with several chemicals at different spatial locations usually requires multiple stamping and registration steps. Here, we describe an experimental method based on reaction–diffusion phenomena that allows for simultaneous micropatterning of a substrate with several coloured chemicals. In this method, called wet stamping (WETS), aqueous solutions of two or more inorganic salts are delivered onto a film of dry, ionically doped gelatin from an agarose stamp patterned in bas relief. Once in conformal contact, these salts diffuse into the gelatin, where they react to give deeply coloured precipitates. Separation of colours in the plane of the surface is the consequence of the differences in the diffusion coefficients, the solubility products, and the amounts of different salts delivered from the stamp, and is faithfully reproduced by a theoretical model based on a system of reaction–diffusion partial differential equations. The multicolour micropatterns are useful as non-binary optical elements, and could potentially form the basis of new applications in microseparations and in controlled delivery.

Conventional surface micropatterning techniques¹ modify the properties of the substrate only at the locations to which a modifying agent—whether chemical² or radiation^{3,4}—is delivered. As a result, the patterning is binary in the sense that it segregates the surface into modified and unmodified regions. For example, soft lithographic methods^{5,6} that use elastomeric stamps deliver chemicals^{7–9} onto the surface only from the raised features of the stamp; the remaining portion of the surface is left unchanged. Micropatterning of surfaces with several chemicals and/or with gradients of chemicals requires either multiple stampings¹⁰ (introducing problems with precise spatial alignment of consecutive patterning steps) or elaborate microfabrication of stamps having complex, three-dimensional structures of the bas relief¹¹. Simple, reliable techniques for non-binary micropatterning would have potential applications in optics^{12–14}, specialized biological assays^{15,16} and biomaterials¹⁷. Our experimental method, based on widely studied reaction–diffusion phenomena^{18–23}, allows simultaneous patterning of salt-doped, transparent films of dry gelatin with different colours at different locations. We use agarose stamps patterned in bas relief and soaked in a mixture of inorganic salts that give coloured precipitates with the salt in the gel²⁴. When the raised features of the stamp are brought into conformal contact with the surface of the dry film, salt solutions diffuse and react (that is, precipitate) in the gelatin matrix. Our method can be used to pattern surfaces with two and in some cases even with three colours. We develop a theoretical model that identifies key parameters controlling colour-separation, and can guide the selection of chemicals appropriate for colour micropatterning.

Figure 1 illustrates the experimental procedure based on wet stamping (WETS) and described in detail elsewhere²⁵. Briefly, an agarose stamp (8 wt% agarose; OmniPur) patterned in bas relief (feature depth 40 μm , typical feature size 50–100 μm) is soaked in a mixture of two or more inorganic salts (typically, 0.25 M to 1.0 M) for 1 hour and brought into conformal contact with a 45- μm -thick layer of dry gelatin doped with 1 wt% of potassium hexacyanoferrate $\text{K}_4[\text{Fe}(\text{CN})_6]$ for 30 minutes. The salts in the stamp are chosen in such a way that their cations react with $[\text{Fe}(\text{CN})_6]^{4-}$ ions to give deeply coloured precipitates. For example, FeCl_3 gives a dark-blue precipitate (Prussian blue), CuCl_2 gives brown, CoCl_2 turquoise and $\text{Er}(\text{NO}_3)_3$ pale blue.

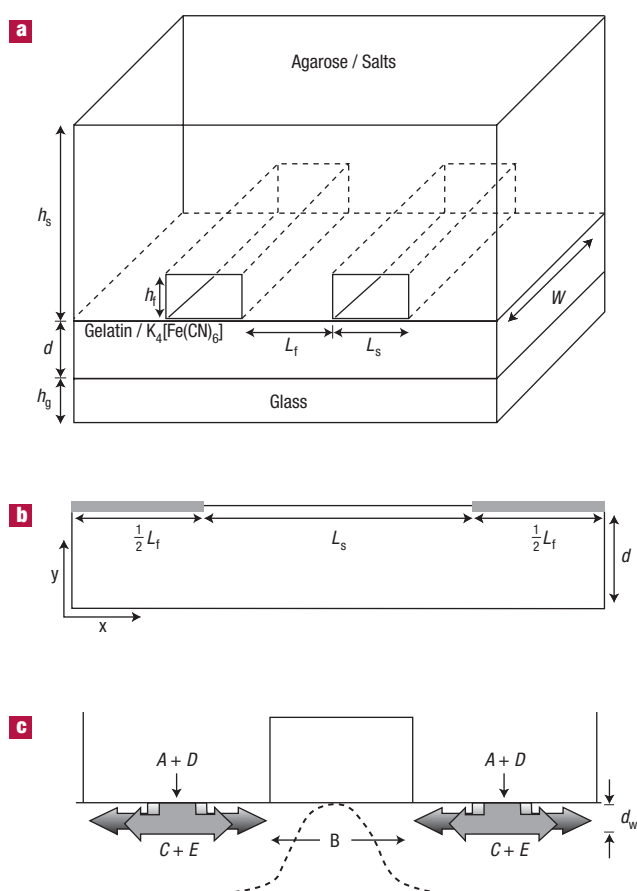


Figure 1 Multicolour patterning of ionically doped gels. **a**, The experimental setup for patterning mixtures of salt solutions (for example, CoCl_2 , CuCl_2 or FeCl_3) onto thin films of dry gelatin doped with $\text{K}_4\text{Fe}(\text{CN})_6$, with typical dimensions of the agarose stamp and of the gelatin layer: $L_s = 50\text{--}250\ \mu\text{m}$, $L_f = 50\text{--}250\ \mu\text{m}$, $h_s = 5\text{--}20\ \text{mm}$, $w = 10\ \text{mm}$, $h_t = 40\ \mu\text{m}$, $d = 45\ \mu\text{m}$, $h_g = 1\ \text{mm}$; where the subscript *s* refers to the spacing of the features in the stamp and the stamp's dimensions, *f* refers to the dimensions of the features, and *g* to those of the glass support. **b**, The geometry of parallel-line features used in the calculations. **c**, Schematic representation of the reaction–diffusion processes that occur after a stamp is brought into conformal contact with the gelatin surface. In the theoretical model described in the text, *A* and *D* are, respectively, Fe^{3+} and Cu^{2+} , *B* stands for $[\text{Fe}(\text{CN})_6]^{4-}$ and *C* and *E* represent the precipitates $\text{Fe}_4[\text{Fe}(\text{CN})_6]_3$ and $\text{Cu}_2[\text{Fe}(\text{CN})_6]$, respectively.

Because the colour difference between the precipitates formed by iron and copper salts was more prominent than for other salt combinations, we used the $\text{FeCl}_3/\text{CuCl}_2$ mixtures as a model system to study colour separation.

Once in conformal contact, water from the stamp rapidly wets the surface of dry gelatin and slowly diffuses into its bulk. Wetting of the surface is driven by capillarity and occurs at a rate of $\sim 1.5\ \mu\text{m}\ \text{s}^{-1}$; the transport of water into the bulk of the gel is a diffusive process against the osmotic pressure due to the immobilized $\text{K}_4[\text{Fe}(\text{CN})_6]$, and is characterized by the diffusion coefficient²⁵ $D_w \approx 10^{-7}\ \text{cm}^2\ \text{s}^{-1}$. When Fe^{3+} and Cu^{2+} carried by water enter the gel, they are instantaneously precipitated in reaction with the $[\text{Fe}(\text{CN})_6]^{4-}$ ions. Local concentrations of metal cations are replenished by their influx from the stamp, but the reaction front (marked by a coloured precipitate) propagates only when all potassium hexacyanoferrate at a given location is used. As a result, the

reaction front travels more slowly (with effective diffusion constant $D_s \approx 10^{-5}\ \text{cm}^2\ \text{s}^{-1}$ similar for both copper and iron ions or fronts) than water swelling the gelatin. In other words, metal cations entering the gel diffuse and react in a thin layer of an already swollen gel near the surface. The thickness of this layer d_w can be estimated from the relation $d_w \approx \sqrt{D_w/D_s}L_s$, where L_s is a characteristic distance travelled by the reaction front (typically, tens of micrometres); with the measured values of the diffusion coefficients, d_w is typically several micrometres.

Iron and copper cations diffuse in the wetted gel precipitate at different locations to give patterns with clearly separated colour zones (Fig. 2). The separation of colours is a result of an intricate interplay between diffusion coefficients of ions in gelatin, their solubility products with respect to the common $[\text{Fe}(\text{CN})_6]^{4-}$ ion, and the local dehydration of agarose in the stamp's features. Each of these factors is discussed in detail below.

DIFFUSION COEFFICIENTS

To estimate relative diffusion coefficients of copper, iron, and hexacyanoferrate(II) in wetted gelatin films and in agarose stamps, we did two sets of experiments.

In gelatin. Two rectangular blocks of agarose soaked in solutions of CuCl_2 and $\text{K}_4[\text{Fe}(\text{CN})_6]$, respectively, were placed parallel to one another and about 0.5 cm apart on a film of dry gelatin. The line where the diffusing Cu^{2+} and $[\text{Fe}(\text{CN})_6]^{4-}$ ions met was marked by precipitate. The ratio of diffusion coefficients, $D_{\text{Cu}^{2+}}:D_{[\text{Fe}(\text{CN})_6]^{4-}}$ was found by taking the ratio of the squares of distances travelled by the ions from the edges of the stamps. A similar experiment with stamps soaked in solutions of FeCl_3 and $\text{K}_4[\text{Fe}(\text{CN})_6]$ yielded the ratio $D_{\text{Fe}^{3+}}:D_{[\text{Fe}(\text{CN})_6]^{4-}}$. Overall, the relative magnitudes of diffusion coefficients of all three species were found to be: $D_{\text{Cu}^{2+}}:D_{\text{Fe}^{3+}}:D_{[\text{Fe}(\text{CN})_6]^{4-}} = 2:1:0.3$ (with a maximal error of the ratios $\sim 20\%$ as estimated from five independent measurements).

In agarose. A rectangular slab of agarose gel with two rectangular wells in its surface (about 1 cm apart) was prepared. One well was filled with a solution of CuCl_2 or FeCl_3 , and the other with a solution of $\text{K}_4[\text{Fe}(\text{CN})_6]$. The ratios of diffusion coefficients were found as before. An important finding is that Cu^{2+} and Fe^{3+} cations had roughly equal diffusion coefficients.

SOLUBILITY PRODUCTS

The solubility products for the iron and copper precipitates are²⁶

$$K_{\text{sp}}^{(1)} = [\text{Fe}^{3+}]^4 [[\text{Fe}(\text{CN})_6]^{4-}]^3 = 3.3 \times 10^{-41}$$

$$K_{\text{sp}}^{(2)} = [\text{Cu}^{2+}]^2 [\text{Fe}(\text{CN})_6]^{4-} = 1.3 \times 10^{-16}$$

That is, iron precipitates more readily than copper.

TRANSFER OF IONS FROM THE STAMP

As the water flows from the features of an agarose stamp into gelatin, a gradient of water content is established²⁵: there is less water near the base of the features than at the bottom (that is, near the gelatin surface). Because the diffusion coefficients of metal cations decrease rapidly with decreasing water content in agarose^{25,27,28} only the cations originally contained in the features can diffuse into gelatin; those originally in the bulk of the stamp cannot be transported into the features through a low-diffusivity, dried region. In other words, the stamping procedure delivers specified amounts of metal cations to the gel.

To prove this hypothesis, we performed the following experiment: a stamp patterned with parallel lines and soaked in a low-concentration (0.1 M) salt solution (either CuCl_2 or FeCl_3) was brought into conformal contact with the gelatin surface and left for a long time ($\sim 1\ \text{h}$). The coloured precipitation zones that formed filled only a small portion (less than 20% in both cases) of the area between the features leaving wide, clear lines between them. Unlike in experiments with more concentrated salt solutions, these clear lines contained unused

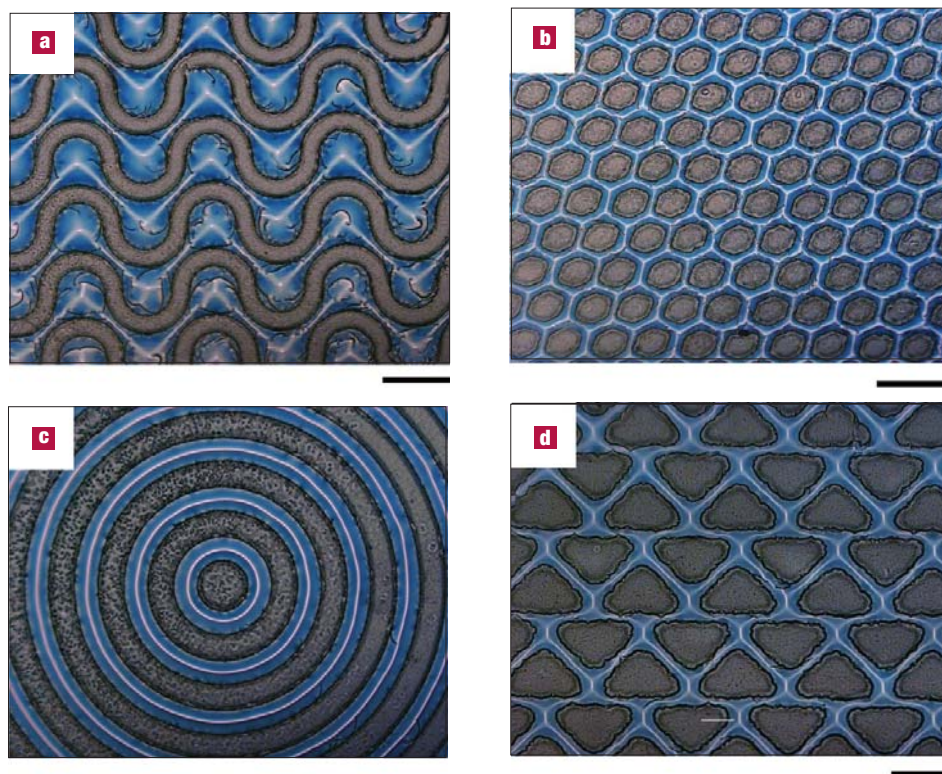


Figure 2 Two-colour patterns in the iron/copper system. In all cases, the stamps were soaked in a mixture of FeCl_3 and CuCl_2 (0.5 M each) for 60 min prior to stamping, and were left in contact with gelatine for 30 min. The scale bars correspond to 200 μm .

$\text{K}_4[\text{Fe}(\text{CN})_6]$ (visualized by flooding the surface with a solution of FeCl_3), indicating that the number of metal cations delivered into the gelatin film was too small to consume all $[\text{Fe}(\text{CN})_6]^{4-}$ therein. This, in turn, means that the flux of cations from the stamp into gelatin must have stopped at some point—otherwise, for sufficiently long times, cations constantly delivered from the agarose would have eventually precipitated all available potassium hexacyanoferrate. These results are consistent with the proposed ‘diffusional closure’ of the features of the stamp.

The effective thickness, h_{eff} , of the agarose layer supplying cations to gelatin can be estimated in the following way. Let L_f and l denote, respectively, the width of the feature in the stamp and the distance travelled by the reaction front from the feature’s edge. The balance of reagents yields $h_{\text{eff}} = svd_w(1 + 2l/L_f)$, where s is a stoichiometric factor (equal to 2 for Cu^{2+} and 4/3 for Fe^{3+}), and v is the ratio of the initial concentration of metal ions in the stamp to that of hexacyanoferrate ions in the gel. For the values of parameters used in experiments, we found that $h_{\text{eff}}^{\text{Fe}^{3+}} \approx 2 h_{\text{eff}}^{\text{Cu}^{2+}} \approx 20 \mu\text{m}$. The observed difference between $h_{\text{eff}}^{\text{Fe}^{3+}}$ and $h_{\text{eff}}^{\text{Cu}^{2+}}$ can be attributed to different permeability of the stamp–gel interface to iron and copper ions, as well as to different sensitivities of the diffusion coefficients to the drying of the gel. The thickness of the agarose layer supplying cations is commensurate with the typical feature height that we used (see Fig. 1).

Based on these experimental observations, the mechanism that explains the formation of the two-colour patterns can be qualitatively described as follows. Once the stamp is in contact with the gel’s surface, copper cations diffuse into gelatin more rapidly than iron cations. Consequently, they react with $[\text{Fe}(\text{CN})_6]^{4-}$ first, and give a layer of brown precipitate under every stamped feature. The iron cations enter a zone

already depleted of $\text{K}_4[\text{Fe}(\text{CN})_6]$. Because the concentration of free Fe^{3+} in this zone is much higher than that of Cu^{2+} , iron cations experience a much higher concentration gradient in the plane of the gelatin film, and thus diffuse outwards from the features more rapidly than copper cations (despite the lower value of the diffusion coefficient of Fe^{3+}). In addition, the flux of copper ions comes to a halt first (because it was initially higher than that of Fe^{3+} , and there are only finite amounts of both types of ions delivered from the drying features of the stamp). The combination of these two effects leads to the diffusion of iron ions eventually ‘overtaking’ that of copper ions, and to the deposition of clean, blue zones of iron precipitate around the brown copper zones (Fig. 2).

We note that the diffusion of both types of cations from nearby features of the stamp towards the region between these features is accompanied by the diffusion of potassium hexacyanoferrate in the opposite direction (Fig. 1c): that is, towards the incoming precipitation fronts. This will be discussed in detail elsewhere. Here, we just briefly mention that the outflow of potassium hexacyanoferrate leads to the formation of clear lines near the centreline between the features. These lines are devoid of $\text{K}_4[\text{Fe}(\text{CN})_6]$; their thickness can be as low as a few hundred nanometres and can be controlled by changing the spacing between the features in the stamp and/or the concentrations of the chemicals used.

To explain the formation of multicolour patterns quantitatively, we consider the process of transferring Fe^{3+} (A in Fig. 1) and Cu^{2+} (D) from an array of parallel, infinite lines in conformal contact with a dry gel containing $[\text{Fe}(\text{CN})_6]^{4-}$ (B); the effective geometry of this system can be reduced to a two-dimensional stamp/gel cross-section (Fig. 1). We denote the width of the features in the stamp by L_f , the distance

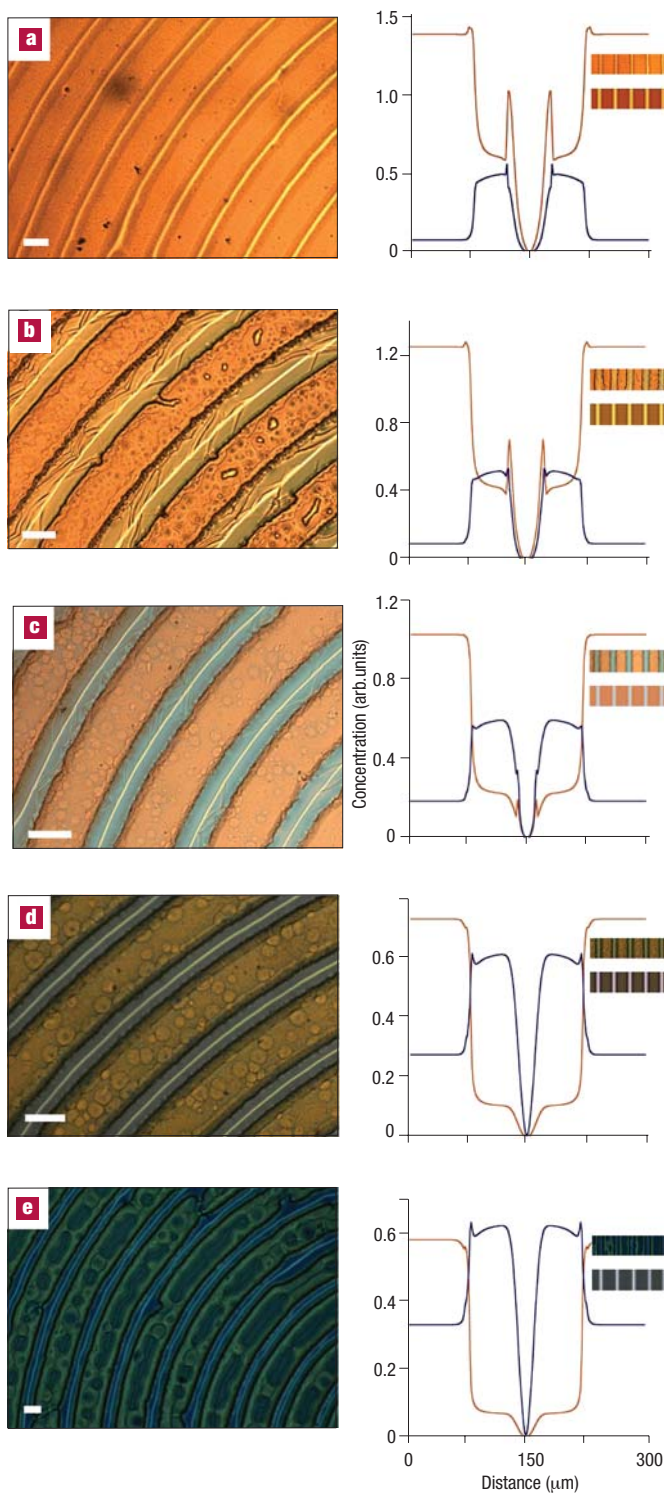


Figure 3 Dependence of colour separation on the relative concentrations of copper and iron salts in the stamp. The left column shows optical micrographs of patterns of concentric circles obtained using mixtures of FeCl_3 and CuCl_2 of different compositions: **a**, 0.25 M FeCl_3 :0.75 M CuCl_2 ; **b**, 0.33 M:0.67 M; **c**, 0.5 M:0.5 M; **d**, 0.67 M:0.33 M; **e**, 0.75 M:0.25 M. All pictures were taken using the same illumination on the Nikon Optiphot 2 microscope interfaced to a Spot 7.4 Slider camera (Diagnostic Instruments). All scale bars correspond to 150 μm . The right column shows the corresponding calculated concentration profiles of $\text{Cu}_2[\text{Fe}(\text{CN})_6]$ (brown lines) and $\text{Fe}_4[\text{Fe}(\text{CN})_6]_3$ (blue lines) between neighbouring circles. Each graph has two colour-stripe inserts: the upper insert is a section of the experimental image; the lower one is obtained from the calculated colour profile. The algorithm for converting concentrations to colour intensities was kindly provided by J. Krupa of Orkla Press. In this algorithm, the concentrations C of brown and blue deposits are first normalized with respect to their maximal values ($C'(x) = (C_{\text{max}}(x) - C(x))/C_{\text{max}}(x)$, where x is the spatial coordinate). These normalized values are then converted to RGB colour components using the formula $R = 255 + \log(C') * (255 - R_{\text{ref}})$, $G = 255 + \log(C') * (255 - G_{\text{ref}})$, $B = 255 + \log(C') * (255 - B_{\text{ref}})$, where R_{ref} , G_{ref} and B_{ref} are the values of pure, saturated brown and blue colours (here, obtained by flooding the surface of doped gelatin with 1 M solutions of either FeCl_3 or CuCl_2). Colour stripes for brown and blue deposits are reconstructed from their RGB components; these stripes are then superimposed onto each other with equal weights.

$$\partial A/\partial t = \nabla(D_A \nabla A) - 4k_1 A^4 B^3$$

$$\partial D/\partial t = \nabla(D_D \nabla D) - 2k_2 D^2 B$$

$$\partial B/\partial t = \nabla(D_B \nabla B) - 4k_1 A^4 B^3 - k_2 D^2 B$$

$$\partial C/\partial t = k_1 A^4 B^3$$

$$\partial E/\partial t = k_2 D^2 B$$

where $D_{A,B,D}$ are, correspondingly, the diffusion coefficients of A , B and D , and $\nabla = \partial/\partial r$ is the two-dimensional gradient operator. As the precipitation reactions are much faster than the transport of components, the reaction terms in the above equations can be treated as precipitation sinks with a threshold determined by the solubility products, $K_{\text{sp}}^{(1)}$ and $K_{\text{sp}}^{(2)}$, and can be mathematically described by the Heaviside step function θ . The use of the Heaviside function implies that if the concentrations of ions are above $K_{\text{sp}}^{(1,2)}$, precipitation occurs instantaneously. With these simplifications, and using dimensionless variables $\tau = tD_A/L_f^2$ and $x = r/L_f$ ($x = (x,y)$), the reaction–diffusion equations take the following form:

$$\partial A/\partial t = D_A^{-1} \nabla(D_A \nabla A) - \delta_A \theta(A^4 B^3 - K_{\text{sp}}^{(1)})$$

$$\partial D/\partial t = D_A^{-1} \nabla(D_D \nabla D) - \delta_D \theta(D^2 B - K_{\text{sp}}^{(2)})$$

$$\partial B/\partial t = D_A^{-1} \nabla(D_B \nabla B) - \delta_{BA} \theta(A^4 B^3 - K_{\text{sp}}^{(1)}) - \delta_{BD} \theta(D^2 B - K_{\text{sp}}^{(2)})$$

$$\partial C/\partial t = \delta_C \theta(A^4 B^3 - K_{\text{sp}}^{(1)})$$

$$\partial E/\partial t = \delta_E \theta(D^2 B - K_{\text{sp}}^{(2)})$$

between them by L_s , and the thickness of the gel layer by d (Fig. 1). We model the process using a reaction–diffusion system of partial differential equations (see Supplementary Information and references therein for the comparison of these equations with those describing related periodic precipitation systems). For the two reactions $4A + 3B \rightarrow C \downarrow$ and $2D + B \rightarrow E \downarrow$ (where C and E stand for $\text{Fe}_4[\text{Fe}(\text{CN})_6]_3$ and $\text{Cu}_2[\text{Fe}(\text{CN})_6]$, respectively, and \downarrow indicates precipitation) the reaction–diffusion equations read

The values of the quantities $\delta_A, \dots, \delta_E$ depend on the concentrations of ions and are calculated in the following way: (1) if the product of A and B is greater than $K_{\text{sp}}^{(1)}$ and the product of D and B is smaller than $K_{\text{sp}}^{(2)}$ —that is, only iron precipitate is formed—then $K_{\text{sp}}^{(1)} = (A - \delta_A)^4 (B - 3\delta_A/4)^3$, $\delta_{BA} = 3\delta_A/4$, $\delta_C = \delta_A/4$ and $\delta_D = \delta_{BD} = \delta_E = 0$; (2) if the product of D and B is greater than $K_{\text{sp}}^{(2)}$ and the product of A and B is smaller than $K_{\text{sp}}^{(1)}$ —only copper precipitates—then $K_{\text{sp}}^{(2)} = (D - \delta_D)^2 (B - \delta_D/2)$, $\delta_{BD} = \delta_E = \delta_D/2$, and $\delta_A = \delta_{BA} = \delta_C = 0$; (3) if both of the concentration products exceed $K_{\text{sp}}^{(1)}$ and $K_{\text{sp}}^{(2)}$ the reactions (1) and (2) occur simultaneously with equal rates (k_1 and k_2) until one of the

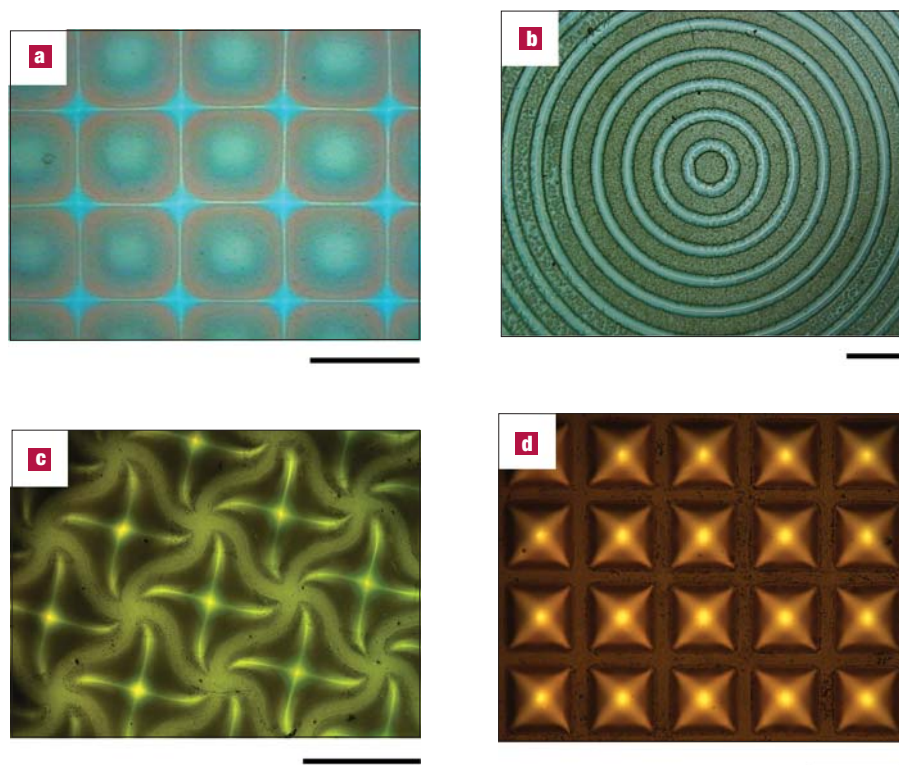


Figure 4 Multicolour and gradient patterns. **a**, A three-colour pattern obtained by using a stamp with a square array of circles embossed on its surface, and soaked in a mixture of CuCl_2 , FeCl_3 , and CoCl_2 (0.014 M:0.31 M:0.67 M). **b**, Concentric circles were patterned with a mixture of FeCl_3 , CuCl_2 and $\text{Er}(\text{NO}_3)_3$ (7%:7%:7% b/w). Pale blue erbium precipitates formed mostly between the stamped circles. Combination of iron and copper deposits gave the greenish-ashen colour below the features. **c, d**, Colour gradient patterns emerging from arrays of wiggly lines (**c**) and perpendicular lines (**d**) were obtained using mixtures of $\text{CoCl}_2/\text{CuCl}_2$ (5%:5% b/w) and $\text{CoCl}_2/\text{FeCl}_3/\text{CuCl}_2$ (5%:5%:5% b/w), respectively.

products reaches its solubility threshold. The quantities $\delta_A, \dots, \delta_E$ are then calculated in two steps. In the first step $\delta_A = \delta_D = \delta$, $\delta_B = 5\delta/4$, $\delta_C = \delta/4$ and $\delta_E = \delta/2$, where $\delta = \min(\delta_1, \delta_2)$, with $K_{\text{sp}}^{(1)} = (A - \delta_1)^4 (B - 5\delta_1/4)^3$, $K_{\text{sp}}^{(2)} = (D - 5\delta_2/4)^2 (B - 5\delta_2/4)$; in the second step, if any of the two concentration products exceeds its solubility threshold, $\delta_A, \dots, \delta_E$ are further updated according to (1) or (2).

We solved the reaction–diffusion equations using the Crank–Nicholson integration scheme²⁹ with the following initial boundary conditions: (1) for the metal cations: $A(x, \tau) = A_0(\tau)$ and $D(x, \tau) = D_0(\tau)$ at the stamp–gel interface ($y = d$ and $0 < x < L_f/2$ and $L_s + L_f/2 < x < L_s + L_f$), and $\nabla A(x) = \nabla D(x) = 0$ for $y = 0$ and for $y = d$ and $L_f/2 < x < L_s + L_f/2$; (2) for the hexacyanoferrate and the precipitates: $B(x, \tau = 0) = B_0$; $C(x, \tau = 0) = E(x, \tau = 0) = 0$; and $\nabla B(x) = \nabla C(x) = \nabla E(x) = 0$ for $y = 0$ and $y = d$. Additionally, we imposed periodic boundary conditions for all concentrations along the x direction. To account for the fact that finite numbers of ions of each kind, $N_{A,D}^0$, are transferred from the stamp into the gel, we applied the following conditions: $A_0(\tau) = A_0$ and $D_0(\tau) = D_0$ if the numbers of ions transferred into the gel until time τ did not exceed N_A^0 and N_D^0 , respectively; and $\nabla A(x) = 0$ or $\nabla D(x) = 0$ at the stamp–gel interface if they did. We assumed that the total number of cations delivered into the gel was $N_A^0 + N_D^0 = (wA_0 + D_0)h_{\text{eff}}$, with the weight $w = 2$, and that the iron and copper ions enter the gel in proportion $N_A^0/N_D^0 = wA_0/D_0$. The weight w accounts for the experimental observation that h_{eff} for Fe^{3+} is about twice that for Cu^{2+} . The input parameters in the simulations were the initial concentrations A_0 , B_0 and D_0 , the ratio of the diffusion coefficients, $D_{A,B,D}^0$, and the thickness h_{eff} . The diffusion coefficients were

assumed to have the following forms: $D_{A,D}(y) = D_{A,D}^0 \eta(y)$ and $D_B(x, y) = D_B^0 \eta(y) \exp[-\alpha(C(x, y) + E(x, y))]$, where α is a constant. The function $\eta(y) = 1$ for $d > y > d - d_w$, and 0 otherwise, accounts for the fact that the ions diffuse only within a thin, wetted surface layer of thickness d_w . The exponential term reflects the experimentally observed^{25,30,31} rapid decrease of the diffusion coefficient of potassium hexacyanoferrate with the increasing local concentrations of precipitates $C(x)$ and $E(x)$.

We solved the system of the reaction–diffusion equations for $D_A^0:D_B^0:D_D^0 = 1:2:0.3$, $L_f = L_s = 150 \mu\text{m}$, $d_w = 8 \mu\text{m}$, $h_{\text{eff}} = 22 \mu\text{m}$, $B_0 = 0.25 \text{ M}$, $K_{\text{sp}}^{(1)} = 3.3 \times 10^{-41}$, $K_{\text{sp}}^{(2)} = 1.3 \times 10^{-16}$. The parameter α was chosen so as to minimize the amount of precipitate in the centreline region; the value of α used in the calculations was 15 M^{-1} .

The predictions of the model are in excellent agreement with experimental results. Figure 3 shows calculated and experimental colour profiles for five different molar concentrations of iron chloride and copper chloride solutions in the agarose stamp (0.75:0.25, 0.67:0.33, 0.5:0.5, 0.33:0.67 and 0.25:0.75). The best colour separation occurs for equal concentrations of the salt, 0.5 M:0.5 M. When iron is present in excess, the areas below and near features are grey-blue, and the space between them is blue. When the stamp has more copper than iron cations, the regions below and near the features are brownish (combination of blue and brown precipitates) and the areas between them are ashen. When solutions are used in which the total salt concentration is lower than 1 M (for example, 0.25 M:0.25 M), the quality of separations is similar, but the hues of the colours are less vivid. In contrast, more concentrated solutions (for example, 1 M:1 M) are impractical to use, as they deform and damage the gelatin film.

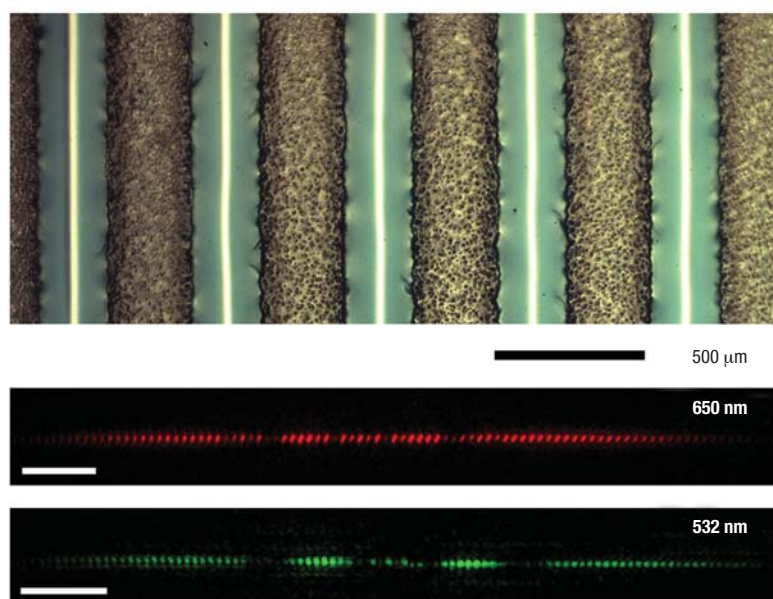


Figure 5 Multicolour patterns as wave-selective diffraction gratings. The top picture is an optical micrograph of a two-colour pattern obtained by stamping an equimolar (0.5 M:0.5 M) solution of FeCl_3 and CuCl_2 . As the brown, blue and clear portions of the gelatin film have different optical characteristics, the coloured gel gives different diffraction patterns with different wavelengths of incident laser light. This effect is illustrated in the middle ($\lambda_1 = 650$ nm) and bottom ($\lambda_2 = 532$ nm) images of diffraction patterns taken 4.5 m from the grating (both scale bars correspond to 5 cm). The differences in the relative intensities of the same diffraction orders in both patterns reflect different absorption of the red and green light by different portions of the multicolour grating. We note that the spacings between diffraction orders are larger in the red pattern than in the green (by a factor of 1.22, in excellent agreement with a theoretical value of $\lambda_1/\lambda_2 = 1.2218$).

We note that changing the amounts of cations delivered to the gel can control the quality of colour separation. These amounts are, in turn, determined by the product of the initial concentrations of ions in the stamp, the surface area of features and their depth. They can thus be adjusted by changing either the concentrations of salts or feature dimensions. We also mention that the experimentally observed colour separation cannot be reproduced by theoretical models that do not account for the finite numbers of cations being delivered to the gelatin. We tested several such models and even with additional assumptions (for example, decrease of the diffusion coefficients of copper with the concentration of precipitate) and/or free parameters, the separations they predicted were, at best, marginal.

Patterns of colours other than blue and brown can be obtained by using different combinations of inorganic salts. Figure 4 shows surfaces patterned in two and even three colours using cobalt, copper, iron and europium salts. Although the number of inorganic salts giving coloured precipitates is large, their diffusion coefficients in agarose and gelatin (or other gels that could be used) need to be measured. At present, the choices of salts to use are somewhat heuristic. But when the necessary data is tabulated, our method (accompanied by modelling) could be used to pattern thin films of gels with, arguably, arbitrary combinations of colours. Such films could be used as wave-selective diffraction gratings (Fig. 5) or gradient photolithographic masks³². Because the reaction–diffusion phenomena responsible for colour separation operate at submicrometre length scales, the accuracy of diffusion-based multicolour patterning would be much better than that of, for instance, ink-jet printing methods. We envisage further uses of our technique in microscale affinity-based separations³³ and in controlled delivery³⁴ applications. In the former area, gels could be doped with a substance having different affinities for several analytes delivered simultaneously from a stamp; if these analytes had different diffusion coefficients in the gel matrix, they should separate spatially. Applications in controlled

delivery would be based on the diffusional closure of the features due to the water outflow from the stamp: the amounts of solute delivered to the gel film could be controlled by changing the area and the depth of the features.

Received 6 February 2004; accepted 31 August 2004; published 19 September 2004.

References

- Choudhury, P. R. (ed.) *Handbook of Microlithography, Micromachining, and Microfabrication* (SPIE, Bellingham, 1997).
- Michel, B. *et al.* Printing meets lithography: Soft approaches to high-resolution printing. *IBM J. Res. Dev.* **45**, 697–719 (2001).
- Tolfree, D. W. L. Microfabrication using synchrotron radiation. *Rep. Prog. Phys.* **61**, 313–351 (1998).
- Thompson, L. F. & Kerwin, R. E. Polymer resist systems for photolithography and electron lithography. *Ann. Rev. Mater. Sci.* **6**, 267–301 (1976).
- Xia, Y. & Whitesides, G. M. Soft lithography. *Angew. Chem. Int. Edn* **37**, 551–575 (1998).
- Xia, Y., Rogers, J. A., Paul, K. E. & Whitesides, G. M. Unconventional methods for fabricating and patterning nanostructures. *Chem. Rev.* **99**, 1823–1848 (1999).
- Delamarche, E. *et al.* Microcontact printing using poly(dimethylsiloxane) stamps hydrophilized by poly(ethylene oxide) silanes. *Langmuir* **19**, 8749–8758 (2003).
- Kind, H. *et al.* Printing gel-like catalysts for the directed growth of multiwall carbon nanotubes. *Langmuir* **16**, 6877–6883 (2003).
- Renault, J. P. *et al.* Fabricating arrays of single protein molecules on glass using microcontact printing. *J. Phys. Chem. B* **107**, 703–711 (2003).
- Rogers, J. A. *et al.* Paper-like electronic displays: Large-area rubber-stamped plastic sheets of electronics and microencapsulated electrophoretic inks. *Proc. Natl Acad. Sci.* **98**, 4835–4840 (2001).
- Tien, J., Nelson, C. M. & Chen, C. S. Fabrication of aligned microstructures with a single elastomeric stamp. *Proc. Natl Acad. Sci.* **99**, 1758–1762 (2002).
- Chen, C., Hirdes, D. & Folch, A. Gray-scale photolithography using microfluidic photomasks. *Proc. Natl Acad. Sci.* **100**, 1499–1504 (2003).
- Frank, M., Schallenberg, U. B. & Kaiser, N. Micropatterned multilayer dielectric filters with two spectral characteristics. *Opt. Eng.* **36**, 1220–1224 (1997).
- Peng, Q. *et al.* Real-time photolithographic technique for fabrication of arbitrarily shaped microstructures. *Opt. Eng.* **42**, 477–481 (2003).
- Fosser, K. A. & Nuzzo, R. G. Fabrication of patterned multicomponent protein gradients and gradient arrays using microfluidic depletion. *Anal. Chem.* **75**, 5775–5782 (2003).
- Dertinger, S. K. W., Jiang, X. Y., Li, Z. Y., Murthy, V. N. & Whitesides, G. M. Gradients of substrate-bound laminin orient axonal specification of neurons. *Proc. Natl Acad. Sci.* **99**, 12542–12547 (2002).
- Wong, J. Y., Velasco, A., Rajagopalan, P. & Pham, Q. Directed movement of vascular smooth muscle cells on gradient-compliant hydrogels. *Langmuir* **19**, 1908–1913 (2003).

18. Hensch, H. K. *Periodic Precipitation* (Pergamon, Oxford, 1991).
19. Turing, A. M. The chemical basis of morphogenesis. *Phil. Trans. R. Soc. B* **237**, 37–72 (1952).
20. Zhabotinsky, A. M. & Zaikin, A. N. Concentration wave propagation in two-dimensional liquid phase self-oscillating system. *Nature* **225**, 535–537 (1970).
21. Lengyel, I. & Epstein, I. R. Modeling of Turing structures in the chlorite–iodide–malonic acid–starch reaction system. *Science* **251**, 650–652 (1991).
22. Ouyang, Q. & Swinney, H. L. Transition from a uniform state to hexagonal and striped Turing patterns. *Nature* **352**, 610–612 (1991).
23. Hess, B. & Mikhailov, A. Self-organization in living cells. *Science* **264**, 223–224 (1994).
24. Bussemas, H. H. & Ertre, L. S. Forerunners of chromatography: Runge's self-grown pictures. *LC GCN. Am.* **22**, 262–270 (2004).
25. Fialkowski, M., Campbell, C. J., Bensemann, I. T. & Grzybowski, B. A. Absorption of water by thin, ionic films of gelatin. *Langmuir* **20**, 3513–3516 (2004).
26. Tananayev, I. V., Glushkova, M. A. & Seifer, B. G. Series of ferrocyanide solubilities. *Zh. Neorg. Khim.* **1**, 66–69 (1956).
27. Valente, A. J. M., Polishchuk, A. Ya., Lobo, V. M. M. & Geuskens, G. Diffusion coefficients of lithium chloride and potassium chloride in hydrogel membranes derived from acrylamide. *Eur. Polym. J.* **38**, 13–18 (2002).
28. Krajewska, B. Diffusion of metal ions through gel chitosan membranes. *Reactive Funct. Polym.* **47**, 37–47 (2003).
29. Ames, W. F. *Numerical Methods for Partial Differential Equations* (Academic, New York 1977).
30. Gao, P. & Fagerness, P. E. Diffusion in HPMC gels. 1. Determination of drug and water diffusivity by pulsed-field-gradient spin-echo NMR. *Pharm. Res.* **12**, 955–964 (1995).
31. Masaro, L. & Zhu, X. X. Physical models of diffusion for polymer solutions, gels and solids. *Prog. Polym. Sci.* **24**, 731–755 (1999).
32. Hantz, P. Regular microscopic patterns produced by simple reaction–diffusion systems. *Phys. Chem. Chem. Phys.* **4**, 1262–1267 (2002).
33. Guzman, N. A. & Stubbs, R. J. The use of selective adsorbents in capillary electrophoresis-mass spectrometry for analyte preconcentration and microreactions: A powerful three-dimensional tool for multiple chemical and biological applications. *Electrophoresis* **22**, 3602–3628 (2001).
34. LaVan, D. A., McGuire, T. & Langer, R. Small-scale systems for in vivo drug delivery. *Nature Biotechnol.* **21**, 1184–1191 (2003).

Acknowledgements

This work was supported by the Northwestern University start-up funds. B.A.G. gratefully acknowledges financial support from the Camille and Henry Dreyfus New Faculty Awards Program. M.F. was supported by the NATO Scientific Fellowship, and C.C. and K.B. by the NSF-IGERT Dynamics of Complex Systems in Science and Engineering Graduate Fellowship. Correspondence and requests for materials should be addressed to B.A.G. Supplementary Information accompanies the paper on www.nature.com/naturematerials

Competing financial interests

The authors declare that they have no competing financial interests.